

# CUEING: A pioneer work of encoding human gaze for autonomous driving

LINFENG LIANG, Macquarie University, Australia

YIRAN WANG, Australian National Univeristy, Australia

YAO DENG, Macquarie University, Australia

JIANCHAO LU, Macquarie University, Australia

CHEN WANG, CSIRO DATA61, Australia

XI ZHENG, Macquarie University, Australia

Recent analysis of incidents involving Autonomous Driving Systems (ADS) has shown that the decision-making process of ADS can be significantly different from that of human drivers. To improve the performance of ADS, it may be helpful to incorporate the human decision-making process, particularly the signals provided by the human gaze. There are many existing works to create human gaze datasets and predict the human gaze using deep learning models. However, current datasets of human gaze are noisy and include irrelevant objects that can hinder model training. Additionally, existing CNN-based models for predicting human gaze lack generalizability across different datasets and driving conditions, and many models have a centre bias in their prediction such that the gaze tends to be generated in the centre of the gaze map. To address these gaps, we propose an adaptive method for cleansing existing human gaze datasets and a robust convolutional self-attention gaze prediction model. Our quantitative metrics show that our cleansing method improves models' performance by up to 7.38% and generalizability by up to 8.24% compared to those trained on the original datasets. Furthermore, our model demonstrates an improvement of up to 12.13% in terms of generalizability compared to the state-of-the-art (SOTA) models. Notably, it achieves these gains while conserving up to 98.12% of computation resources.

CCS Concepts: • **Human-centered computing** → **Ubiquitous and mobile computing design and evaluation methods**.

Additional Key Words and Phrases: autonomous driving, human attention, gaz map, convolution attention models

## ACM Reference Format:

Linfeng Liang, Yiran Wang, Yao Deng, Jianchao Lu, Chen Wang, and Xi Zheng. 2023. CUEING: A pioneer work of encoding human gaze for autonomous driving. In *Proc. ACM Interact. Mob. Wearable Ubiquitous Technol.*. ACM, New York, NY, USA, 19 pages. <https://doi.org/10.1145/nnnnnnn.nnnnnnn>

## 1 INTRODUCTION

End-to-end autonomous driving is a self-contained driving system in which inputs from sensors such as Inertial Measurement Unit (IMU), camera LiDAR, radar, and GPS are directly fed into the neural networks for vehicle control prediction, such as the steering wheel turning angle, the acceleration, and additional actions the automobile should undertake next [21, 23]. However, recent research has demonstrated that the predicted control behaviour of Tesla's autonomous driving differs dramatically from that of experienced human drivers [32], which challenges the trustworthiness of the decision-making of such systems. Intuitively, during the driving process, drivers determine how to control the car based on the road circumstances observed visually. Integrating human knowledge into autonomous driving systems holds

---

Permission to make digital or hard copies of all or part of this work for personal or classroom use is granted without fee provided that copies are not made or distributed for profit or commercial advantage and that copies bear this notice and the full citation on the first page. Copyrights for components of this work owned by others than ACM must be honored. Abstracting with credit is permitted. To copy otherwise, or republish, to post on servers or to redistribute to lists, requires prior specific permission and/or a fee. Request permissions from [permissions@acm.org](mailto:permissions@acm.org).

© 2023 Association for Computing Machinery.

Manuscript submitted to ACM



Fig. 1. Camera Images from BDD-A (first column), Gaze map from BDD-A (second column), Cleansed gaze map from BDD-A (third column).

great promise [5, 6]. One major research direction is to understand how human drivers recognize and handle dangerous situations [7], with the aim of enabling autonomous driving systems (ADS) to exhibit similar levels of attention as experienced human drivers [1, 16]. Recent research has demonstrated that utilizing eye-tracking data from human drivers can effectively predict their attention for some driving scenarios [13, 25, 28, 35]. Moreover, integrating human attention into an end-to-end autonomous driving system (ADS) has the potential to significantly enhance the system’s ability to accurately predict driving actions [2, 10, 34].

However, despite the availability of extensive gaze data and the development of gaze prediction models [12, 13, 25, 28, 35], recent research findings [18, 24] suggest that the approach of using eye-tracking to capture drivers’ attention poses certain challenges. Specifically, it has been observed that human attention can be easily diverted towards irrelevant items during the driving process [1], and such unrelated gaze data (*Challenge 1*) can have a detrimental effect on the training of gaze prediction models. Figure 1 indicates a comparison between the original gaze map in BDD-A [35] (Column 2) and its cleansed version (Column 3). We can see that, although attempts have been made to collect the average gaze from multiple drivers [35], unrelated gaze (e.g., building, tree and poles) still widely exists in the BDD-A dataset compared to our cleansed version [35].

Furthermore, the gaze prediction models shall have good generalizability when applied to diverse driving scenarios. However, developing an effective gaze prediction model for a new environment often mandates the collection of extensive driving gaze data, which can be costly and time-consuming. Thus, another major challenge lies in the development of a more generalizable gaze prediction model that can perform well across diverse scenarios (*Challenge 2*). In the pursuit of a generalizable prediction model, prior research has revealed a centre bias in many gaze prediction models. This bias causes the generated gaze to predominantly concentrate in the centre area of the gaze map [24, 28]. The presence of a centre bias can be both advantageous and problematic. Human drivers naturally focus on the centre of the front while driving, which aligns with intuitive behaviour. However, if the centre bias is excessively strong, all gaze predictions tend to be concentrated in the centre. The influence of centre bias on the generalizability of gaze prediction models remains uncertain.

To tackle these challenges, we propose a pipeline that aims to filter out unrelated gaze data present in current datasets, allowing the model to focus specifically on driving-related objects during training. Additionally, we introduce

a novel convolutional self-attention gaze prediction model that enhances generalizability by concentrating on important semantic objects, while also considering the correlation among different subfields in the input image to prevent the occurrence of centre bias. Through our experiments, we have effectively addressed both challenges (*Challenges 1 and 2*), while also minimizing the computational resources required for the attention model. In summary, our contributions can be outlined as follows:

- **Cleansing method:** We propose an adaptive pipeline to cleanse gaze prediction datasets, and allow different gaze prediction models trained on those cleansed datasets to achieve better results.
- **Model:** We present a novel convolutional self-attention gaze prediction model that exhibits enhanced generalizability compared to existing gaze prediction models.
- **Experiments:** We conduct extensive experiments to evaluate our cleansing method and model against the state-of-the-art and provide insights for future research directions.

This paper is organized as follows: In section 2, we provide a review and discussion of the related work relevant to our study. Sections 3 and 4 detail how we created our dataset and model, respectively. In section 5, we indicate the design of our experiments. In section 6, we present the results of our comprehensive experiments based on the methodology described in sections 3 and 4. In section 7, we discuss potential threats against our proposed methods.

## 2 RELATED WORK

Previous studies have introduced several gaze prediction datasets. Dr(eye)VE [3] consists of videos collected from real-world driving scenarios though with a smaller number of road users. BDD-A [35] primarily focuses on critical driving situations and employs in-lab methods to collect averaged gaze data from 20 drivers, which was gathered in San Francisco. Similarly, DADA-2000 [12] is generated using in-lab methods and comprises video clips depicting 54 different types of accidents across various environments. The dataset was collected in China, where cultural and road conditions differ from previous datasets. Additionally, CDNN [9] is collected in a similar way to DADA-2000. To counter the noise collected from eye-tracking equipment [1, 18], Xia et al. [35] used multiple drivers' averaged attention data as the ground truth in their work. However, as shown in Figure 1, some ground truth gaze still focus on unrelated objects such as the sky or trees. In another related work, Pal et al. [24] integrated the label and embedding information of related objects into the ground truth to remove labelling noises. However, this pre-processed ground truth gaze map is very different from a real human gaze map. In their method, they used Mask-RCNN [14] to capture specific objects such as vehicles and pedestrians in the image. In comparison, our cleansing method leveraged the existing semantic labels in the given dataset to extract the bounding boxes of the most critical semantic objects. By masking all the other pixels, we were able to create a more accurate and focused gaze map. The experiments demonstrate that our gaze map successfully focuses on specific objects that are highly relevant to driving scenarios.

In terms of gaze prediction models, Previous research primarily focuses on designing gaze prediction models using pre-trained CNN backbones, such as AlexNet [35], Yolo [28], or VGG [29]. This approach can be seen as mapping the extracted features to ground-truth gaze. Additionally, a grid-based gaze prediction method has been proposed, which divides the input into grids and predicts gaze for each grid [28]. These methods have achieved decent quantitative results. Another approach, CDNN [9], provides a gaze predictor without a backbone but requires downsizing the original inputs. A major issue in these prior works is their heavy reliance on CNNs, which have limitations in capturing the relationships among different subfields in the input images. The gaze prediction task actually requires capturing these relationships effectively. Furthermore, previous models often require image pre-processing, either through feature

extraction or downsizing. In contrast, our approach offers a model with significantly lower computation resources, as it is not heavily reliant on convolution filters and does not require a pre-trained backbone. Instead, our model employs a tokenization method similar to the vision transformer (ViT) [11], enabling the use of self-attention mechanisms to capture the relationships among subfields. Compared to recent gaze prediction approaches that utilize inverse reinforcement learning [4], our method does not require a range of prior labels involving relative distance, driving tasks, vehicle state, and road information, which can be challenging to obtain, especially across diverse datasets.

### 3 DATASET CLEANSING

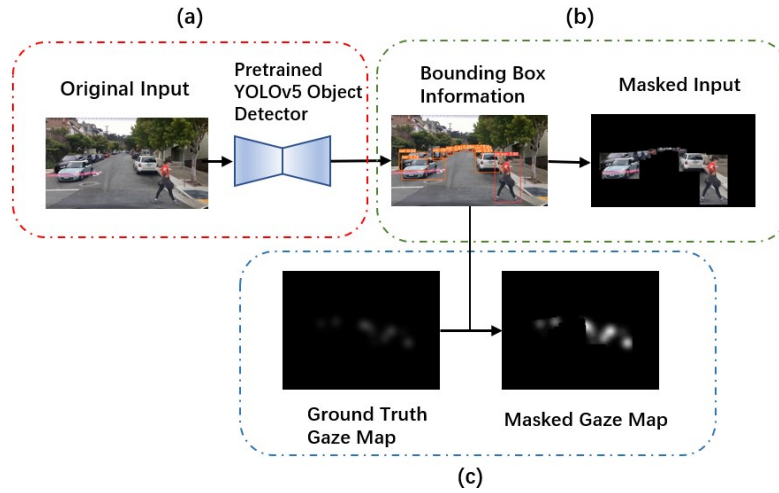


Fig. 2. Dataset Cleansing Process.

We propose a pipeline for cleansing the existing driving attention datasets, as illustrated in Figure 2. In Figure 2 (a), we first use a pre-trained YOLOv5 [15] object detector to obtain the bounding box information from the original inputs, the detail of this part is included in Section 3.1. Subsequently, using this detection model, we can generate masked inputs (Figure 2 (b)) and masked gaze maps (Figure 2 (c)) by applying bounding box-specified masks to the original images and gaze maps, the detail of this part is included in Section 3.2.

#### 3.1 Unrelated Gaze

Unlike commonly used datasets such as ImageNet [8] or COCO [20], labels and inputs in gaze maps do not align well. The ground truth collected from human drivers contains bias, and such bias also happens in the process of human attention ground truth collection [1, 18]. Currently, the major method to collect human attention is to use eye-tracking equipment, drivers' attention can be drawn by unrelated objects, which could hinder the effectiveness of the collected data for training the model. Here, we define 'unrelated gaze' as the collected attention that is not directly related to the driving activity. For example, if a driver's attention is not focused on an object or the focused object that is not related to driving, we regard this part of gaze as noise. To distinguish between related and unrelated objects, we utilize objects' labels and embedding information in the scene. BDD-100K [36] provides object detection labels for 10 important objects for driving-related tasks including pedestrian, rider, car, truck, bus, train, motorcycle, bicycle, traffic light, and

traffic sign. Such semantic labels can be obtained in gaze datasets. In order to do so, we fine-tuned an object detection model YOLOv5 [15] to extract the bounding boxes information of objects corresponding to these semantic labels in our cleansing method. With the bounding box information, we can then remove the unrelated gaze from the original gaze map (Figure 2 (a)).

### 3.2 Masked Input and Ground Truth

Many CNN or ViT [11] based feature extraction methods extract features from the entire input image without considering the difference in importance of image segments in terms of the semantic labels of these segments. In the context of gaze prediction, certain image segments hold more significance than others. For example, objects like vehicles and pedestrians carry more meaningful information for driving scenarios compared to irrelevant elements like the sky or trees. Therefore, once we have obtained the prior semantic information, we can treat non-critical objects in the current scenario as noise. In our cleansing method, we utilize the bounding box information to identify and select critical semantic information, while masking out all other pixels (Figure 2 (b)).

Apart from embedding information, the spatial location of semantic objects is also crucial in the original inputs. Our cleansing method intends to retain as much location information as possible while removing unnecessary semantic information. In addition to modifying the input, we also process the ground truth gaze map to eliminate labeling noise (e.g., gaze focused on the sky or trees). To accomplish this, we apply the bounding box technique to the original gaze map, selecting only the gaze information located inside the bounding box for meaningful semantic objects (Figure 2 (c)).

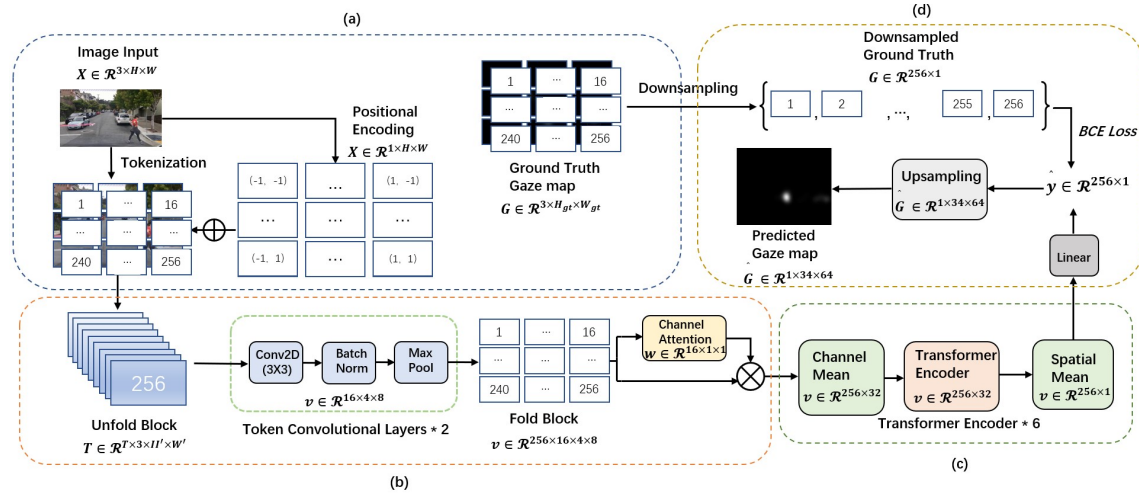


Fig. 3. Overview of our proposed CUEING Model Architecture.

## 4 CUEING MODEL

An overall model architecture is shown in Figure 3. The first step is to conduct tokenization and positional encoding on original inputs, and then downsample the ground truth gaze map (Figure 3 (a)). After that, to further extract information from these tokens, we stack up these tokens and apply token convolutional layers (Figure 3 (b)) and the transformer

encoders on them (Figure 3 (c)). Finally, we calculate the loss and upsample the output of the linear layer to visualize the gaze map (Figure 3 (d)).

#### 4.1 Tokenization

Predicting the attention in a grid-based style achieves decent results in the gaze prediction task [28]. However, they use a convolutional layer with kernel size  $1 \times 1$  to map the extracted feature to the array of gaze values, which does not fully exploit the advantages of the 'grid-based' style. In our model, we apply a 'token-to-point' approach to improve this i.e. we tokenize original inputs from driving scenarios  $X \in \mathcal{R}^{3 \times H \times W}$  to  $X \in \mathcal{R}^{T \times 3 \times H' \times W'}$  where  $H$  and  $W$  refer to the height and width of original input and  $T$  is the number of tokens which is 256 by default, and the number is empirically evaluated against multiple datasets. Since there is the same number of tokens in each row and column, then  $H' = H/\sqrt{T}$  and  $W' = W/\sqrt{T}$ . Specifically, similar to convolution, we first use a non-parameterized sliding window that has the same size as the token to move through the input from the left-top to right-bottom without any overlap to form tokens. We call this operation *tokenization*. Different from convolution, we do not sum the information in each token, but we stack them up in a batch. The operation is called *unfold*. The process is illustrated in Figure 3(a). After applying these operations, the inputs are turned into a stack of tokens. The motivation for our tokenization is to map a series of tokens to a series of points, those points represent the strength of gaze that is likely to be mapped in each token. Then we downsample the ground truth gaze map into points using a similar idea with tokenization. Differently, after we receive the tokens from the ground truth gaze map, we calculate an average gaze value for each token in the ground truth as the 'point'. The ground truth gaze map is then downsampled from  $G \in \mathcal{R}^{3 \times H_{gt} \times W_{gt}}$  to  $G \in \mathcal{R}^{T \times 1}$  with the number of points equal to the number of tokens. The number of points is 256 by default. The downsampled ground truth will be used to calculate the loss (Figure 3 (d)). In our model, we do not apply normal convolution operation on the original inputs. The first reason is to avoid the limitation of the receptive field in CNN. Secondly, our input size is  $1280 \times 720$  and we produce 256 tokens by default as the approach of ViT [11]. We tried to avoid high-channels and large kernel convolutional layers which are expensive in computation. Then, in order to extract the feature in each token, we use token convolution and positional encoding.

#### 4.2 Positional Encoding

Due to the tokenisation and the following token convolution and attention blocks, we assign each token a specific positional in the original input (Figure 3 (a)). To obtain accurate positional information on tokens, we would prefer that the location information could be feature-like information in the original input. Therefore the location information can be further processed as a feature by convolutional layers in the next stage. Here we employ a specifically designed absolute positional encoding, we assign a two-dimensional coordinate to each token, and these coordinates will equally spread between -1 and 1 through the rows and columns. For example, we tokenize an input into  $3 \times 3$  tokens, the first token has coordinates  $(-1, -1)$ , while the coordinates to its right will be  $(0, -1)$  and the coordinates below it will be  $(-1, 0)$  (Figure 4). Hence, we can ensure that each token in the original input has a unique coordinate. However, to allow the positional information could be the same dimension as the features of the token, we use a convolutional layer map the two-dimensional encoded coordinate from  $P \in \mathcal{R}^{2 \times H \times W}$  to  $P \in \mathcal{R}^{1 \times H \times W}$  and then add it to each pixel in the token as  $X = P + X$ , where  $X$  is the original token.

$(-1, -1)$	$(0, -1)$	$(1, -1)$
$(-1, 0)$	$(0, 0)$	$(1, 0)$
$(-1, 1)$	$(0, 1)$	$(1, 1)$

Fig. 4. Example of Positional Encoding

### 4.3 Token Convolution

To do token convolution, we stack all the tokens from a single input into a batch, which is indicated as the first step of (b) in Figure 3. Therefore, the dimension in this stage reduce from  $\mathcal{R}^{T \times 3 \times H' \times W'}$  to  $\mathcal{R}^{3 \times H' \times W'}$ . Then, we use the two convolutional layers with a kernel size of  $3 \times 3$  to downsize the tokens and shrink channels to 16 (Figure 3 (b)). After the token convolution, we need to put those stacked tokens into their original place for further processing, and this is the operation we call fold in Figure 3 (b). In this step the dimension of the feature map  $v$  will be increased from  $\mathcal{R}^{16 \times 4 \times 8}$  to  $\mathcal{R}^{T \times 16 \times 4 \times 8}$ . However, in order to allow self-attention blocks can process our tokens, we either need to merge channels or feature size of produced feature map  $v$  to 1, as after the attention blocks, the quantitative value of feature maps that could produce gaze will become closer. Therefore, we choose to process the channel dimension before the attention block. Here we employ channel attention [33] to the output of the convolutional layer to assign each channel a trainable weight i.e.  $v = v \otimes w$ , where  $w$  is the weight of channels. By applying weight to each channel, then we average the channel dimension, and the feature's dimension is reduced from  $\mathcal{R}^{T \times 16 \times 4 \times 8}$  to  $\mathcal{R}^{T \times 4 \times 8}$ .

### 4.4 Attention Between Tokens

Generally, if we simplify the gaze prediction problem into a binary classification problem, i.e., the gazed areas are white, and other areas are black, the relationship between tokens will not be captured. Under our settings, the relationship between tokens is important, after the attention layer. Ideally, pixels that could generate gaze should become similar before feeding into a linear layer. Therefore, we use transformer encoders [31] for our model. Specifically, we use 6 symmetric self-attention layers to find the attention scores between tokens, since we want to capture the relationship between all the tokens (Figure 3 (c)). We validate the importance of attention blocks in our ablation study in Section 6.3.1. Looking back to the positional encoding, it is not only for the convolutional layers to learn the position feature of each feature but also could work as an absolute positional encoding for transformer encoders. After the transformer encoders, in order to allow the output can be processed by linear layer, we used a spatial mean in each token to reduce the dimension, then the dimension is reduced from  $\mathcal{R}^{T \times 32}$  to  $\mathcal{R}^{T \times 1}$  under our default setting, we use the output from linear layer to calculate the loss, and the loss function here we used is Binary Cross Entropy loss. Finally, to visualize the gaze map, we use interpolation and Gaussian smoothing to upsample the output from the linear layer to form the final gaze map (Figure 3 (d)).

## 5 EXPERIMENT

We proposed four research questions (RQs) and conducted corresponding experiments to evaluate the effectiveness of our proposed model and cleansed datasets:

- RQ1: Can our cleansed datasets produce more reasonable human gaze than the baseline dataset?
- RQ2: Can our cleansed datasets improve the performance of the gaze prediction models than the baseline datasets?
- RQ3: Can our model have better generalizability and performance than other gaze prediction models?
- RQ4: Can removing centre bias improve the generalizability of gaze prediction models?

To evaluate our RQs, we cleansed two large and popular datasets BDD-A [35] and DADA-2000 [12] datasets and produced two cleansed datasets CUEING-B and CUEING-D. We resized all inputs into  $1280 \times 720$  which is aligned with the initial size of BDD-A [35] input. For RQ1, we conducted a user study to compare the BDD-A [35] with the CUEING-B and the DADA-2000 [12] with the CUEING-D. BDD-A [35] and CUEING-B contain 30,073 images, and DADA-2000 [12] and CUEING-D contain 22,171 images. To ensure a 95% confidence level with a 10% confidence interval, we randomly sampled 100 images with gaze maps from both original datasets and their cleansed version respectively. In those sampled groups, to gain quantitative measurement, we let users decide how many clusters of gaze each image contains, and how many of them are reasonable. For example, in Figure 4, the left image has 4 clusters of gaze and 1 of them are unreasonable, and the right image has 2 cluster of gaze and all of them are reasonable. We recruited 10 workers in mTurk to participate in the user study, and all of them are car owners and have extensive driving experience. They can receive 1\$ for each survey they take, we made 5 surveys in total. During the user study, we did not instruct users on how to alter their subconscious, users need to rely entirely on their subjective perceptions to determine which image contains more reasonable gaze.



Fig. 5. Example of user study interface, the left side is the overlay of image and gaze map from DADA-2000, the right side is the overlay of image and gaze map from CUEING-D.

For RQ2 and RQ3, our experiment involved several large and popular datasets as baselines including Dr(eye)VE [3], BDD-A [35], and DADA-2000 [12], which were collected under different conditions. We also compare our cleansed

datasets with another augmented driving gaze dataset SAGE [24], we used the SAGE [24] method to augment BDD-A [35] and produced SAGE-B [24] to compare with our cleansing method. To evaluate our cleansing method, we follow the principle 'training on synthetic and testing on real [27, 30]' to keep a fair comparison. For example, if we want to evaluate CUEING-B or SAGE-B [24], then we train the models on the dataset and then test the models using a separate real-world dataset set (testing set in BDD-A [35]). In model selection, we included CUEING model and the latest and popular gaze prediction models, including HWS [35], CDNN [9], Where&What [28]. To evaluate the performance of our cleansing method and model, we divided the evaluation metrics into three parts: object detection (object-level), saliency map generation (pixel-level) and computation resources required. To compare the quality of generated gaze maps, we used the Kullback–Leibler divergence ( $D_{KL}$ ) and Pearson's Correlation Coefficient ( $CC$ ) metrics as in previous works [28, 35]. Similarly, we resized the predicted and ground-truth saliency maps to  $36 \times 64$ , keeping the original width and height ratio following the setting of [28] to have a fair comparison. For the object-level, we want to measure the difference between the generated gaze map and the ground truth gaze map in terms of focusing on 'what' objects detected by YOLOv5 [15] similar to other visual attention-based object detection tasks [19, 22, 28]. Therefore, the evaluation of the object-level performance is conducted using standard machine learning metrics, including Accuracy, Precision, Recall, F1, and AUC. In order to determine whether an object is considered 'focused on,' we define a threshold criterion based on the gaze predictions within the bounding box of the detected object. Following the approach used in [28], if the maximum predicted gaze value within the bounding box exceeds the threshold of 0.5, the object is deemed as being focused on by the driver. This threshold is independent of the training and pixel-level metrics and is used primarily for object-level evaluation. To compare the computational resources required, we employ the same metrics as in [28], which include the number of trainable parameters in the model and the number of floating-point operations per second for a single input (GFLOPS). These metrics provide a standardized measure for assessing the computational efficiency of different models.

For RQ3, we assessed the generalizability of the models through two approaches. Firstly, we considered a model to exhibit higher generalizability if it was trained on a source dataset and achieved better performance on a target dataset. Secondly, we defined a model as having higher generalizability if it was trained on a source dataset and demonstrated improved results after fine-tuning using a small portion (2% of the total training data) from the target dataset. In our experiments, we employed CUEING-B, BDD-A [35], and CUEING-D, DADA-2000 [12] as the source datasets, while DADA-2000, Dr(eye)VE, and BDD-A were used as the target datasets. To evaluate the second approach, we randomly sampled images from the target datasets (DADA-2000 [12] and Dr(eye)VE [3]) for CUEING-B and BDD-A [35] (as source datasets), and from BDD-A [35] (as target dataset) for CUEING-D and DADA-2000 [12] (as source datasets) to fine-tune the pre-trained models. The performance evaluation was conducted using the same metrics as in RQ2, ensuring consistency in the evaluation process.

For RQ4, center bias is a known phenomenon observed in gaze prediction tasks [24, 28]. When the center bias is strong, the trained model consistently outputs gaze towards the center of the gaze map, regardless of the actual focus of attention. We formulated a hypothesis that the center bias impacts model generalizability. To validate this hypothesis, we first introduced a metric to quantify the degree of center bias, enabling us to obtain a quantitative understanding of this phenomenon. To measure the level of center bias, we utilized models trained on the original datasets as well as their corresponding cleansed versions. Using the corresponding testing set, we generated gaze maps using each model and aggregated them by summing the predicted gaze values at each pixel location. Next, we calculated the mean of the summed gaze maps, taking into account the number of generated gaze maps. Normalizing the averaged gaze map allowed us to obtain a normalized averaged gaze map, in which the maximum value represents the gaze divergence,

denoted as  $I$ . A higher gaze divergence indicates a more pronounced center bias in the gaze generator, while a lower value indicates less bias towards the center. By quantifying the gaze divergence, we can effectively measure the severity of center bias in different gaze models, thereby investigating its impact on model generalizability.

$$I_d = \max\left(\frac{1}{n} \sum_{j=1:n} \|\hat{G}_j\|\right) \quad (1)$$

where  $d$  refers to the name of the gaze model (e.g., CUEING trained on CUIENG-B and HWS trained on BDD-A),  $n$  refers to the total number of generated gaze maps, and  $\hat{G}_j \in \mathcal{R}^{36 \times 64}$  refer to the generated gaze map. For this research question, we compared BDD-A [35] with CUEING-B and DADA-2000 [12] with CUEING-D on all baseline models.

Our implementation is based on Pytorch [26] and used the Adam optimizer [17], and all our experiments are done on an RTX 3090 GPU.

## 6 RESULTS

### 6.1 User Study (RQ1)

To process our collected user study results from mTurk, we first calculated the mean value using the answers from all users for each question, we then used these mean values to find the ratio of reasonable gaze in each image, and finally, we Min-Max normalised the ratio from the original dataset and its cleansed version to obtain the quantitative results. Figure 6 indicates the quantitative result of our user study. We can see that users consider the datasets that have used our cleansing method (red and green) to contain more reasonable gaze than their corresponding original datasets (blue and yellow) in both medians and mean.

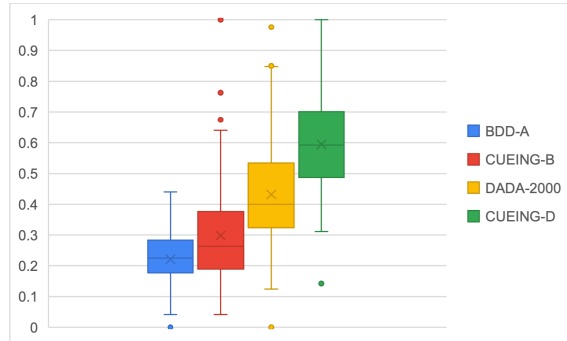


Fig. 6. Quantitative result of the user study, the order of the boxes in the figure is BDD-A, CUEING-B, DADA-2000, CUEING-D (left to right).

Here we further explore the reasons for the outliers in Figure 6. In Figure 7, we present some examples of outliers. The first row is the example from DADA-2000 and CUEING-D, the right image is from CUEING-D, and it contains no gaze after cleansing. This leads to a limitation of our cleansing method, because we are using the available semantic labels from BDD-100K [36] to train the YOLOv5 [15] model, this means the objects that can be detected limited by the availability of semantic labels in BDD-100K [36]. In this instance it is reasonable for the driver to look on the bushes in this circumstance, but bush is not in the BDD-100K's [36] semantic label set. This points out to an interesting future research work where we can generate a diverse semantic label sets after processing a number of existing gaze datasets.

The second and third rows in Figure 7 display examples from BDD-A [35] and CUEING-B. In the second row, the left image from BDD-A [35] demonstrates a scenario where both datasets fail to detect the white car, despite it being the object of focus for most drivers in similar situations. However, it's important to note that this image represents a single frame from the video, and it's possible that the driver may have shifted their attention to the car later in the video. This highlights the significance of incorporating time series data in gaze prediction rather than relying solely on individual frames. Previous research has indicated that integrating time series data at this stage does not enhance performance and may introduce significant centre bias [28]. As a potential future direction, training a robust gaze attention model on videos is essential.

The third row indicates that after the cleansing process, a significant portion of the gaze is removed from the original image. While most of the removed gaze does not contain useful information, the right turn mark on the street holds value. This observation raises an intriguing direction for future research, which involves incorporating specific street signs into our semantic object datasets, not only those on the street sides but also those present on the street or hanging in the air.



Fig. 7. Outlier examples, the first row is from DADA-2000 (left) and CUEING-D (right), second and third rows are from BDD-A (left) and CUEING-B (right).

## 6.2 Cleansing Method (RQ2)

Table 1 and 2 list the object and pixel-level metrics of baseline models. Our cleansed datasets do not significantly improve the  $D_{KL}$  and  $CC$  performance since our cleansing method was not designed for pixel-level metrics. However, most models trained by our cleansed datasets have different levels of improvement in object-level metrics. In the gaze prediction task, because of the positive and negative sample balance, we believe Accuracy, F1 and AUC are more

important than other object-level metrics. Intuitively, the level of improvement is dependent on the dataset i.e. if the dataset contains more unrelated gaze, then the improvement will be more significant. For example, we can see the improvement of AUC and Accuracy in DADA-2000 [12] is more significant, this is because DADA-2000 [12] is collected from a single driver and contain more unrelated gaze, while BDD-A [35] is the averaged gaze from multiple drivers, which contains less unrelated gaze. Therefore, the improvement of our cleansing method on BDD-A [35] is less than on DADA-2000 [12]. On the other hand, under the principle of 'training on synthetic and testing on real', the performance of SAGE-B [24] is significantly worse than the performance of CUEING-B, but it is worth noting that the recalls of the models trained on SAGE-B [24] are very high. This is because SAGE [24] almost includes all objects' labels and embedding from the input in their ground truth, which is rare across different gaze datasets. Figure 8 indicates a comparison between the generated gaze map using CUEING model trained by SAGE-B [24] and CUEING-B, the gaze map generated by the model trained by SAGE-B is quite different from real human's gaze. Therefore, SAGE [24] tends to capture all objects in the input instead of focusing on the important objects, which hinders the generalizability of the models. As a future direction, we plan to assess the significance of gaze map generalizability in co-training essential driving models, such as perception.

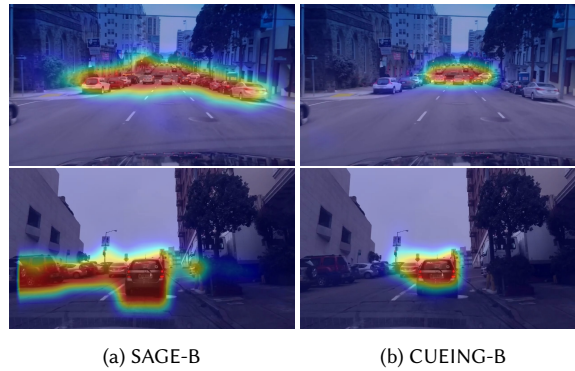


Fig. 8. Example of prediction results generated by CUEING model train on SAGE-B (left) and CUEING-B (right).

Model	Object Level(CUEING-B/BDDA/SAGE-B)					Pixel Level(CUEING-B/BDDA/SAGE-B)	
	Acc(%)	Prec(%)	Recall(%)	F1(%)	AUC	KL	CC
CDNN	53.48/53.57/38.76	44.27/44.35/37.74	97.26/97.77/99.78	60.85/61.02/54.77	0.84/0.85/0.60	2.26/4.89/2.26	0.35/0.05/0.22
Where&What	78.11/78.04/53.42	67.60/69.75/44.93	72.19/72.27/90.46	69.70/70.99/60.05	0.84/0.85/0.63	1.35/1.15/1.87	0.55/0.60/0.34
HWS	57.19/64.24/49.65	46.21/51.08/41.91	92.54/88.87/91.92	61.64/64.88/57.57	0.78/0.81/0.62	1.80/1.69/2.38	0.49/0.54/0.28
CUEING	77.39/76.27/59.10	71.64/67.73/47.17	68.84/69.22/81.86	70.21/68.47/59.44	0.84/0.83/0.68	1.56/1.31/1.89	0.54/0.55/0.34

Table 1. Selected Models' performance on BDD-A testing set, and the best result is bold.

### 6.3 Generalizability and General Performance of CUEING model (RQ3)

In terms of the overall performance of our model, Table 1 and 2 demonstrate that CUEING exhibits a notable difference of 12% in pixel-level performance compared to the current state-of-the-art models (e.g., Where&What [28]). When considering object-level metrics, our model is either slightly inferior or even superior to the existing state-of-the-art models. This indicates that our model achieves our design goal in capturing important objects of attention.

Model	Object Level(CUEING-D/DADA-2000)					Pixel Level(CUEING-D/DADA-2000)	
	Acc(%)	Prec(%)	Recall(%)	F1(%)	AUC	KL	CC
CDNN	41.18/ <b>47.04</b>	25.89/ <b>25.94</b>	<b>84.74</b> /71.45	<b>39.66</b> /38.06	0.58/ <b>0.59</b>	5.13/ <b>2.89</b>	0.05/ <b>0.10</b>
Where&What	<b>85.14</b> /78.89	46.81/ <b>63.14</b>	<b>65.71</b> /65.54	54.67/ <b>64.32</b>	<b>0.87</b> /0.84	2.53/ <b>2.11</b>	0.31/ <b>0.38</b>
HWS	<b>47.16</b> /45.79	25.04/ <b>25.43</b>	66.04/ <b>71.45</b>	36.32/ <b>37.51</b>	0.55/ <b>0.57</b>	9.16/ <b>3.53</b>	0.02/ <b>0.09</b>
<b>CUEING</b>	<b>85.80</b> /78.42	48.42/ <b>52.50</b>	<b>62.12</b> /57.04	54.42/ <b>54.68</b>	<b>0.87</b> /0.80	2.78/ <b>2.20</b>	0.28/ <b>0.36</b>

Table 2. Selected Models' performance on CUEING-D and DADA-2000 datasets, and the best result is bold.

Furthermore, Table 6 presents the evaluation metrics for the computation resources required by the evaluated gaze models. Notably, our model achieves these impressive results while utilizing only 1.8% of the computation resources required by Where&What [28]. This highlights the significant advantage of our model in terms of both computational efficiency and performance compared to other existing models.

In Tables 3, 4, and 5, we present the evaluation of model generalizability by training models on the original datasets and the cleansed datasets, and testing them on DADA-2000 [12], Dr(eye)VE [3], and BDD-A [35] as target datasets, respectively. In the case of DADA-2000 (as the target dataset) [12], we also included SAGE-B [24] in the generalizability experiment.

In terms of model generalizability, our CUEING model consistently outperforms other state-of-the-art models, both with and without fine-tuning. For example, in Table 3, the accuracy of CUEING reaches 80.59% when fine-tuning with a portion of DADA-2000 data, while other models like CDNN and HWS only achieve around 53% and 51% accuracies, respectively. Furthermore, in terms of pixel-level performance, the CUEING model surpasses the current state-of-the-art (e.g., Where&What [28]) by up to 12.13% (KL value of 2.10 versus 2.39). Similar trends can be observed in Tables 4 and 5.

Furthermore, our cleansing method significantly enhances the generalizability of various models, improving both object and pixel-level metrics. When DADA-2000 [12] is used as the target dataset, most models trained on our cleansed dataset show improved performance, even without fine-tuning. For instance, training our CUEING model on the cleansed dataset leads to a further 4.11% improvement in pixel-level performance. Similar improvements are observed in other gaze models, such as HWS [35], which achieves up to a 50.43% improvement in pixel-level performance.

However, there are still some unexpected results that caught our attention. For example, in all three datasets, almost all object-level metrics of HWS [35] decreased after applying our cleansing method, meanwhile, the results indicate that the HWS model has the worst generalizability [35] of all the models. In this case, we believe the generalizability may relate to the centre bias that exists in the human gaze dataset and we discussed this in Section 6.4.

Generalizability Result on DADA-2000								
Model	Object Level(CUEING-B/BDD-A/SAGE-B)					Pixel Level(CUEING-B/BDD-A/SAGE-B)		
	Acc(%)	Prec(%)	Recall(%)	F1(%)	AUC	KL	CC	
CDNN*	<b>53.24</b> /36.93/35.71	27.54/24.84/25.01	64.58/87.37/ <b>91.18</b>	38.62/38.68/ <b>39.24</b>	<b>0.60</b> /0.53/0.58	<b>2.66</b> /3.52/3.13	0.21/0.16/ <b>0.10</b>	
Where&What*	78.18/ <b>79.51</b> /78.57	52.28/ <b>55.49</b> /53.05	50.04/51.58/ <b>53.12</b>	51.14/ <b>53.46</b> /53.09	0.78/ <b>0.79</b> /0.78	2.39/ <b>2.35</b> /2.40	<b>0.32</b> /0.33/0.33	
HWS*	<b>51.11</b> /42.87/48.17	25.06/25.19/ <b>25.93</b>	57.40/ <b>76.36</b> /68.75	34.88/ <b>37.89</b> /37.66	0.55/0.56/ <b>0.58</b>	<b>2.83</b> /5.71/4.30	<b>0.16</b> /0.08/0.07	
<b>CUEING*</b>	<b>80.59</b> /78.71/77.99	<b>57.63</b> /52.98/51.99	56.37/ <b>59.55</b> /46.11	<b>56.99</b> /56.08/48.87	<b>0.82</b> /0.80/0.77	<b>2.10</b> /2.19/2.97	<b>0.36</b> /0.35/0.28	
CDNN†	<b>39.96</b> /36.80/25.02	<b>25.29</b> /24.84/23.16	83.73/87.65/ <b>98.88</b>	<b>38.85</b> /38.71/37.53	0.56/0.53/ <b>0.59</b>	3.15/3.15/ <b>2.99</b>	<b>0.08</b> /0.05/0.03	
Where&What†	<b>60.14</b> /55.13/50.20	26.56/24.42/ <b>27.34</b>	42.32/46.16/ <b>71.33</b>	32.64/31.94/ <b>39.52</b>	0.62/0.56/ <b>0.69</b>	3.76/ <b>3.36</b> /3.63	0.08/ <b>0.09</b> /0.07	
HWS†	40.25/ <b>46.29</b> /34.19	24.25/ <b>25.34</b> /24.13	76.21/69.55/ <b>88.11</b>	36.79/37.14/ <b>37.8</b>	0.56/0.55/ <b>0.59</b>	4.62/4.62/ <b>4.44</b>	0.11/ <b>0.13</b> /0.02	
<b>CUEING†</b>	<b>72.13</b> /58.67/49.85	<b>33.39</b> /24.73/26.16	22.22/39.70/ <b>65.73</b>	26.68/30.48/ <b>37.42</b>	<b>0.61</b> /0.56/0.59	3.77/ <b>3.65</b> /3.73	0.06/ <b>0.07</b> /0.04	

Table 3. Model's performance by using CUEING-B, BDD-A and SAGE-B as source datasets Fine-tuned with DADA-2000 as target dataset, and the best result is bold.

\* indicates that the model is fine-tuned on the corresponding dataset, † informs the direct prediction without fine-tuning.

Model	Object Level(CUEING-B/BDD-A)					Pixel Level(CUEING-B/BDDA)	
	Acc(%)	Prec(%)	Recall(%)	F1(%)	AUC	KL	CC
CDNN*	50.62/ <b>52.17</b>	45.12/ <b>45.92</b>	<b>98.80</b> /98.72	61.96/ <b>62.68</b>	0.85/ <b>0.86</b>	<b>2.07/2.07</b>	<b>0.41/0.40</b>
Where&What*	<b>79.55</b> /79.45	73.83/ <b>73.87</b>	<b>77.17</b> /76.87	<b>75.46</b> /75.34	<b>0.87/0.87</b>	1.55/ <b>1.54</b>	<b>0.57/0.57</b>
HWS*	61.20/ <b>65.91</b>	51.31/ <b>54.96</b>	<b>91.00</b> /89.90	65.62/ <b>68.21</b>	0.79/ <b>0.83</b>	<b>2.40/3.30</b>	0.50/ <b>0.43</b>
<b>CUEING*</b>	<b>78.92</b> /78.41	<b>75.50</b> /73.19	71.65/ <b>74.38</b>	<b>73.52/73.78</b>	<b>0.85/0.85</b>	<b>1.69/1.71</b>	<b>0.53/0.53</b>
CDNN†	51.01/ <b>55.45</b>	45.31/ <b>47.69</b>	<b>98.54</b> /98.20	62.07/ <b>64.20</b>	0.76/ <b>0.86</b>	<b>2.41/1.96</b>	0.28/ <b>0.44</b>
Where&What†	74.67/ <b>76.54</b>	65.83/ <b>67.98</b>	78.99/ <b>80.46</b>	71.81/ <b>73.70</b>	0.82/ <b>0.85</b>	1.89/ <b>1.76</b>	0.49/ <b>0.50</b>
HWS†	58.89/ <b>67.09</b>	49.70/ <b>56.11</b>	86.15/ <b>87.77</b>	63.04/ <b>68.45</b>	0.73/0.82	<b>4.33/2.96</b>	0.24/ <b>0.46</b>
<b>CUEING†</b>	<b>63.17/75.85</b>	<b>57.78/67.99</b>	<b>36.49/77.24</b>	<b>44.74/72.32</b>	0.66/ <b>0.83</b>	<b>2.95/1.88</b>	0.21/ <b>0.48</b>

Table 4. Model’s performance by using CUEING-B and BDD-A as source datasets Fine-tuned by Dr(eye)VE as target dataset, and the best result is bold.

\* indicates that the model is fine-tuned on the corresponding dataset, † informs the direct prediction without fine-tuning.

Model	Object Level(CUEING-D/DADA-2000)					Pixel Level(CUEING-D/DADA)	
	Acc(%)	Prec(%)	Recall(%)	F1(%)	AUC	KL	CC
CDNN*	<b>54.10</b> /54.09	<b>44.59</b> /44.58	96.90/ <b>96.94</b>	61.07/ <b>61.08</b>	<b>0.82/0.82</b>	<b>1.67/1.67</b>	<b>0.43/0.43</b>
Where&What*	<b>75.83</b> /75.73	<b>67.02</b> /66.95	<b>68.87</b> /68.53	<b>67.93</b> /67.73	<b>0.83/0.82</b>	<b>1.38/1.41</b>	<b>0.55/0.54</b>
HWS*	64.94/ <b>67.40</b>	51.93/ <b>54.29</b>	77.10/ <b>78.09</b>	62.06/ <b>64.05</b>	0.74/ <b>0.77</b>	<b>2.12/2.14</b>	<b>0.43/0.40</b>
<b>CUEING*</b>	<b>75.00</b> /72.21	<b>68.04</b> /65.59	<b>61.72</b> /53.04	<b>64.73</b> /58.65	<b>0.81/0.77</b>	<b>1.53/2.15</b>	0.49/0.40
CDNN†	46.01/ <b>52.40</b>	40.70/ <b>43.70</b>	<b>99.05</b> /97.35	57.69/ <b>60.32</b>	<b>0.81/0.81</b>	<b>1.84/1.97</b>	<b>0.38/0.35</b>
Where&What†	<b>58.13</b> /58.00	<b>38.36</b> /37.49	<b>20.86</b> /19.49	<b>27.02</b> /25.65	0.59/ <b>0.62</b>	2.95/ <b>2.80</b>	<b>0.10/0.09</b>
HWS†	<b>62.95</b> /58.41	<b>50.98</b> /46.53	<b>92.60</b> /79.59	58.68/ <b>58.73</b>	0.57/ <b>0.69</b>	<b>2.11/3.79</b>	<b>0.30/0.03</b>
<b>CUEING†</b>	57.17/ <b>58.10</b>	34.82/ <b>37.63</b>	17.48/ <b>19.38</b>	23.28/ <b>25.58</b>	0.57/ <b>0.59</b>	<b>2.98/3.13</b>	<b>0.09/0.08</b>

Table 5. Model’s performance by using CUEING-D and DADA-2000 as source datasets Fine-tuned by BDD-A as target dataset, and the best result is bold.

\* indicates that the model is fine-tuned on the corresponding dataset, † informs the direct prediction without fine-tuning.

Model	Param.(M)	GFLOPs
CDNN	0.68	5.06
Where&What	7.52	17.0
HWS	3.75	21.18
<b>CUEING</b>	<b>0.14</b>	<b>0.31</b>

Table 6. Computation resource of different gaze prediction models, and the best result is bold.

**6.3.1 Generalizability Study.** The CUEING model has decent generalizability, but the model is BlackBox, we want to understand which part of the model benefits the generalizability most. Therefore, we conduct an ablation study in generalizability. We compare the results from freezing all layers before the last linear layer and freezing all attention blocks in the CUEING model trained by CUEING-B.

From table 7, we can find that the performance decreased for the model trained on the CUEING-B dataset is larger than the model trained on BDD-A [35] under all the settings. This is because when we generalize our model to DADA-2000 [12], we do not apply masks on the input of DADA-2000 [12], and the distribution of the input data is different from the CUEING-B dataset largely. Therefore, from the result of CUEING model trained on the BDD-A [35] dataset, we

Freeze Block	KL	CC
All except Linear*	2.49	0.29
Attention Module*	2.35	0.32
None of the layers*	2.10	0.38
All except Linear†	2.28	0.34
Attention Module†	2.23	0.35
None of the layers†	2.19	0.36

Table 7. Ablation Study on Generalizability of CUEING Model

† indicates that the model is trained via BDD-A, \* informs it is trained via CUEING-B Dataset.

find that if we transfer our model under similar distribution, only allowing the last linear can be trained can reach a similar result with training all the parameters, which only has a 2.67% increase on the KL-divergence. From the result of CUEING model trained on CUEING-B dataset, we can find that even if we allow all the blocks other than attention blocks for training, the KL-divergence still increase by 11.11% than allowing all the parameters can be trained. Apparently, attention blocks play an important role in our model.

#### 6.4 Centre Bias Study (RQ4)

Tables 8 and 9 present the gaze divergence for various combinations of model and dataset ( $I_{gt}$  refers to the gaze divergence in the ground truth gaze map). A higher gaze divergence indicates that the gaze is concentrated in a central area with a higher centre bias, while a lower gaze divergence suggests a more dispersed gaze with a lower centre bias. After training the models on our cleansed datasets, we observed a significant decrease in gaze divergence compared to the original datasets. For instance, the HWS model trained on DADA-2000 showed a 90.74% decrease in gaze divergence when trained on CUEING-D, and similar behavior was observed for other models. Furthermore, the models trained on our cleansed datasets (CUEING-B and CUEING-D) exhibited better generalizability. These findings support our hypothesis that lower center bias leads to improved generalizability for gaze models. The reason behind this is that our cleansing method tends to remove gaze points around the center. As shown in the third row of Figure 7, although the right image may appear unreasonable to humans, it effectively reduces center bias.

We observed that different models exhibit varying resistances to center bias, even when trained on the same dataset. In terms of generalizability, we found that the Where&What model [28] trained on the higher center bias dataset BDD-A tends to have lower generalizability to the lower center bias dataset DADA-2000 [12]. On the other hand, our CUEING model, trained on BDD-A and applied to DADA-2000, shows better generalizability. This indicates that the CUEING model, leveraging tokenization and attention mechanisms instead of traditional CNN, excels in capturing relationships between different objects, thereby enhancing its ability to resist center bias.

Figure 9 is the prediction results from selected models trained through BDD-A [35] and CUEING-B. Qualitatively, we can find that the CUEING and HWS [35] produce more dispersed gaze, while the Where&What [28] and CDNN [9] produce more concentrated gaze in the centre. Meanwhile, models trained on our cleansed dataset produce more dispersed gaze.

In conclusion, our findings demonstrate that center bias has a significant impact on the performance and generalizability of gaze models. While it is intuitive to assume that human drivers tend to focus on the center of the road while driving, it is equally important to consider other dynamic semantic objects on the road, such as pedestrians preparing to cross or a vehicle merging into the center lane. The CUEING model exhibits lower gaze divergence compared to

Model-Dataset	$I_d$	$I_d - I_{gt}$
Where&What - BDD-A	0.69	0.43
BDD-A model - BDD-A	0.38	0.12
<b>CUEING</b> - BDD-A	0.72	0.46
CDNN - BDD-A	0.87	0.61
Ground Truth - BDD-A	0.26	0.00
Where&What - CUEING-B	0.53	0.39
BDD-A model - CUEING-B	0.28	0.14
<b>CUEING</b> - CUEING-B	0.44	0.31
CDNN - CUEING-B	0.82	0.69
Ground Truth - CUEING-B	0.14	0.00

Table 8. Gaze divergence of models trained on BDD-A and CUEING-B.

Model-Dataset	$I_d$	$I_d - I_{gt}$
Where&What - DADA-2000	0.83	0.65
BDD-A model - DADA-2000	0.33	0.14
<b>CUEING</b> - DADA-2000	0.75	0.57
CDNN - DADA-2000	1.00	0.82
Ground Truth - DADA-2000	0.18	0.00
Where&What - CUEING-D	0.61	0.54
BDD-A model - CUEING-D	0.08	0.01
<b>CUEING</b> - CUEING-D	0.28	0.22
CDNN - CUEING-D	0.63	0.56
Ground Truth - CUEING-B	0.06	0.00

Table 9. Gaze divergence of models trained on DADA-2000 and CUEING-D.

the state-of-the-art model Where&What [28] in the context of gaze prediction. In our future work, we aim to further investigate the importance of eliminating center bias in training mission-critical driving models.

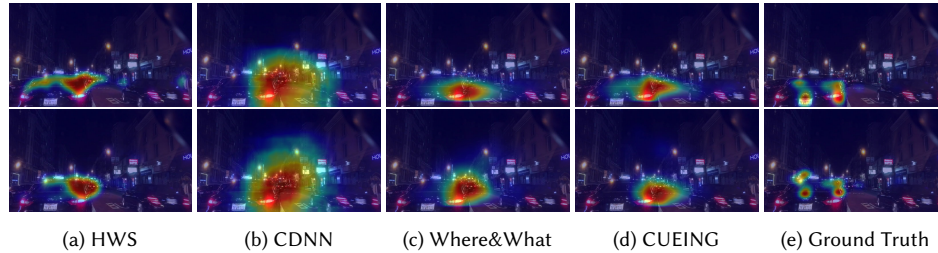


Fig. 9. Example of prediction result by different models through the training of the CUEING-B dataset (first row) and BDD-A dataset (second row).

## 7 THREAT TO VALIDITY

### 7.1 External Validity

The main threat to external validity is regarding the generalization of the proposed method. To address the problem, We conduct experiments on large-scale datasets including BDD-A [35], DADA-2000 [12], SAGE [24], and Dr(eye)VE [3]. The experimental results demonstrate that our cleansing method is effective across these datasets. Furthermore, the new gaze model trained on the additional cleanSed dataset also achieves good performances on other datasets, which shows the generalizability of our method.

### 7.2 Construct Validity

The primary threat to construct validity is related to the evaluation of our method in generating more reasonable gaze maps compared to other existing methods. To address this, we conducted a human study using scale-based rating for gaze clustering, as there are no established quantitative metrics available. To ensure the authenticity of participants' responses, we specifically recruited individuals with driving experience, as the task is directly related to driving and their expertise can reflect realistic actions during driving scenarios.

Regarding the selection of baselines, while we included several baseline datasets, there is one additional driving attention dataset that we did not incorporate, namely CDNN [9]. This dataset is relatively small and collected under similar conditions to DADA-2000 [12]. Additionally, we did not include MEDIRL [4], which is another respectable gaze prediction model, in our baselines. The reason is that MEDIRL is based on inverse reinforcement learning, utilizes video as input, and relies on a substantial amount of prior information such as Relative Distance and Road Information for training, which is not available in the evaluated datasets.

Another potential threat to internal validity is the use of the YOLOv5 [15] model in our cleansing method. We opted for YOLOv5 because it has demonstrated effectiveness and accuracy in object detection tasks, allowing us to extract semantic information from driving images to enhance the identification of reliable gaze maps. However, there is a challenge associated with fine-tuning YOLOv5, as it requires annotations of objects in driving images. Nonetheless, this challenge is more relevant to the datasets themselves rather than the model itself.

## 8 CONCLUSION

In this paper, we present a novel approach that addresses the challenges of data labelling noises and the lack of generalization in gaze models. Our proposed method includes an adaptive dataset cleansing technique and a convolutional self-attention gaze prediction model, both of which effectively mitigate these challenges. The results from our extensive experiments demonstrate the efficacy of our approach.

Furthermore, our work opens up interesting research avenues for future exploration. For example, the development of robust gaze models could involve leveraging video data captured from multiple cameras and incorporating non-traditional semantic objects in driving scenes, such as turning marks on the street. Additionally, it would be valuable to investigate the qualitative and quantitative impact of a generalizable gaze model and a cleaned gaze dataset on driving models. This close-loop step of encoding human knowledge into autonomous driving models could have significant implications.

## REFERENCES

- [1] Christer Ahlström, Katja Kircher, Marcus Nyström, and Benjamin Wolfe. 2021. Eye tracking in driver attention research—how gaze data interpretations influence what we learn. *Frontiers in neuroergonomics* 2 (2021), 778043.
- [2] Ekrem Aksoy, Ahmet Yazıcı, and Mahmut Kasap. 2020. See, Attend and Brake: An Attention-based Saliency Map Prediction Model for End-to-End Driving. *arXiv preprint arXiv:2002.11020* (2020).
- [3] Stefano Alletto, Andrea Palazzi, Francesco Solera, Simone Calderara, and Rita Cucchiara. 2016. Dr (eye) ve: a dataset for attention-based tasks with applications to autonomous and assisted driving. In *Proceedings of the IEEE conference on computer vision and pattern recognition workshops*. 54–60.
- [4] Sonia Bae, Erfan Pakdamanian, Inki Kim, Lu Feng, Vicente Ordonez, and Laura Barnes. 2021. MEDIRL: Predicting the Visual Attention of Drivers via Maximum Entropy Deep Inverse Reinforcement Learning. In *2021 IEEE/CVF International Conference on Computer Vision (ICCV)*. 13158–13168. <https://doi.org/10.1109/ICCV48922.2021.01293>
- [5] Michael Barz, Sebastian Kapp, Jochen Kuhn, and Daniel Sonntag. 2021. Automatic recognition and augmentation of attended objects in real-time using eye tracking and a head-mounted display. In *ACM Symposium on Eye Tracking Research and Applications*. 1–4.
- [6] Felipe Codevilla, Matthias Müller, Antonio López, Vladlen Koltun, and Alexey Dosovitskiy. 2018. End-to-end driving via conditional imitation learning. In *2018 IEEE International Conference on Robotics and Automation (ICRA)*. IEEE, 4693–4700.
- [7] Mark Colley, Svenja Krauss, Mirjam Lanzer, and Enrico Rukzio. 2021. How should automated vehicles communicate critical situations? a comparative analysis of visualization concepts. *Proceedings of the ACM on Interactive, Mobile, Wearable and Ubiquitous Technologies* 5, 3 (2021), 1–23.
- [8] Jia Deng, Wei Dong, Richard Socher, Li-Jia Li, Kai Li, and Li Fei-Fei. 2009. Imagenet: A large-scale hierarchical image database. In *2009 IEEE conference on computer vision and pattern recognition*. Ieee, 248–255.
- [9] Tao Deng, Hongmei Yan, Long Qin, Thuyen Ngo, and BS Manjunath. 2019. How do drivers allocate their potential attention? driving fixation prediction via convolutional neural networks. *IEEE Transactions on Intelligent Transportation Systems* 21, 5 (2019), 2146–2154.
- [10] Jiqian Dong, Sikai Chen, Shuya Zong, Tiantian Chen, and Samuel Labi. 2021. Image transformer for explainable autonomous driving system. In *2021 IEEE International Intelligent Transportation Systems Conference (ITSC)*. IEEE, 2732–2737.

- [11] Alexey Dosovitskiy, Lucas Beyer, Alexander Kolesnikov, Dirk Weissenborn, Xiaohua Zhai, Thomas Unterthiner, Mostafa Dehghani, Matthias Minderer, Georg Heigold, Sylvain Gelly, et al. 2010. An image is worth 16x16 words: Transformers for image recognition at scale. arXiv 2020. *arXiv preprint arXiv:2010.11929* (2010).
- [12] Jianwu Fang, Dingxin Yan, Jiahuan Qiao, Jianru Xue, He Wang, and Sen Li. 2019. Dada-2000: Can driving accident be predicted by driver attentionf analyzed by a benchmark. In *2019 IEEE Intelligent Transportation Systems Conference (ITSC)*. IEEE, 4303–4309.
- [13] Jianwu Fang, Dingxin Yan, Jiahuan Qiao, Jianru Xue, and Hongkai Yu. 2021. DADA: Driver attention prediction in driving accident scenarios. *IEEE Transactions on Intelligent Transportation Systems* 23, 6 (2021), 4959–4971.
- [14] Kaiming He, Georgia Gkioxari, Piotr Dollár, and Ross Girshick. 2017. Mask r-cnn. In *Proceedings of the IEEE international conference on computer vision*. 2961–2969.
- [15] Glenn Jocher, Alex Stoken, Jirka Borovec, NanoCode012, ChristopherSTAN, Liu Changyu, Laughing, tkianai, Adam Hogan, lorenzomamma, yxNONG, AlexWang1900, Laurentiu Diaconu, Marc, wanghaoyang0106, ml5ah, Doug, Francisco Ingham, Frederik, Guilhen, Hatovix, Jake Poznanski, Jiacong Fang, Lijun Yu, changyu98, Mingyu Wang, Naman Gupta, Osama Akhtar, PetrDvoracek, and Prashant Rai. 2020. *ultralytics/yolov5: v3.1 - Bug Fixes and Performance Improvements*. <https://doi.org/10.5281/zenodo.4154370>
- [16] Jinkyu Kim, Anna Rohrbach, Trevor Darrell, John Canny, and Zeynep Akata. 2018. Textual explanations for self-driving vehicles. In *Proceedings of the European conference on computer vision (ECCV)*. 563–578.
- [17] Diederik P Kingma and Jimmy Ba. 2014. Adam: A method for stochastic optimization. *arXiv preprint arXiv:1412.6980* (2014).
- [18] Iuliia Kotseruba and John K Tsotsos. 2022. Attention for Vision-Based Assistive and Automated Driving: A Review of Algorithms and Datasets. *IEEE Transactions on Intelligent Transportation Systems* (2022).
- [19] Niharika Kumari, Verena Ruf, Sergey Mukhametov, Albrecht Schmidt, Jochen Kuhn, and Stefan Küchemann. 2021. Mobile eye-tracking data analysis using object detection via YOLO v4. *Sensors* 21, 22 (2021), 7668.
- [20] Tsung-Yi Lin, Michael Maire, Serge J. Belongie, Lubomir D. Bourdev, Ross B. Girshick, James Hays, Pietro Perona, Deva Ramanan, Piotr Doll’ a r, and C. Lawrence Zitnick. 2014. Microsoft COCO: Common Objects in Context. *CoRR* abs/1405.0312 (2014). arXiv:1405.0312 <http://arxiv.org/abs/1405.0312>
- [21] Congcong Liu, Yuying Chen, Lei Tai, Haoyang Ye, Ming Liu, and Bertram E. Shi. 2019. A Gaze Model Improves Autonomous Driving. In *Proceedings of the 11th ACM Symposium on Eye Tracking Research & Applications (Denver, Colorado) (ETRA ’19)*. Association for Computing Machinery, New York, NY, USA, Article 33, 5 pages. <https://doi.org/10.1145/3314111.3319846>
- [22] Eduardo Manuel Silva Machado, Ivan Carrillo, Miguel Collado, and Liming Chen. 2019. Visual attention-based object detection in cluttered environments. In *2019 IEEE SmartWorld, Ubiquitous Intelligence & Computing, Advanced & Trusted Computing, Scalable Computing & Communications, Cloud & Big Data Computing, Internet of People and Smart City Innovation (SmartWorld/SCALCOM/UIC/ATC/CBDCOM/IOP/SCI)*. IEEE, 133–139.
- [23] Alexander Makrigiorgos, Ali Shafti, Alex Harston, Julien Gerard, and A Aldo Faisal. 2019. Human visual attention prediction boosts learning & performance of autonomous driving agents. *arXiv preprint arXiv:1909.05003* (2019).
- [24] Anwesan Pal, Sayan Mondal, and Henrik I Christensen. 2020. " Looking at the right stuff"-Guided semantic-gaze for autonomous driving. In *Proceedings of the IEEE/CVF Conference on Computer Vision and Pattern Recognition*. 11883–11892.
- [25] Andrea Palazzi, Davide Abati, Francesco Solera, Rita Cucchiara, et al. 2018. Predicting the Driver’s Focus of Attention: the DR (eye) VE Project. *IEEE transactions on pattern analysis and machine intelligence* 41, 7 (2018), 1720–1733.
- [26] Adam Paszke, Sam Gross, Francisco Massa, Adam Lerer, James Bradbury, Gregory Chanan, Trevor Killeen, Zeming Lin, Natalia Gimelshein, Luca Antiga, Alban Desmaison, Andreas Kopf, Edward Yang, Zachary DeVito, Martin Raison, Alykhan Tejani, Sasank Chilamkurthy, Benoit Steiner, Lu Fang, Junjie Bai, and Soumith Chintala. 2019. PyTorch: An Imperative Style, High-Performance Deep Learning Library. In *Advances in Neural Information Processing Systems* 32. Curran Associates, Inc., 8024–8035. <http://papers.neurips.cc/paper/9015-pytorch-an-imperative-style-high-performance-deep-learning-library.pdf>
- [27] Xingchao Peng, Ben Usman, Neela Kaushik, Dequan Wang, Judy Hoffman, and Kate Saenko. 2018. Visda: A synthetic-to-real benchmark for visual domain adaptation. In *Proceedings of the IEEE Conference on Computer Vision and Pattern Recognition Workshops*. 2021–2026.
- [28] Yao Rong, Naemi-Rebecca Kassautzki, Wolfgang Fuhl, and Enkelejda Kasneci. 2022. Where and What: Driver Attention-based Object Detection. *Proceedings of the ACM on Human-Computer Interaction* 6, ETRA (2022), 1–22.
- [29] Karen Simonyan and Andrew Zisserman. 2015. Very Deep Convolutional Networks for Large-Scale Image Recognition. arXiv:1409.1556 [cs.CV]
- [30] Gul Varol, Javier Romero, Xavier Martin, Naureen Mahmood, Michael J Black, Ivan Laptev, and Cordelia Schmid. 2017. Learning from synthetic humans. In *Proceedings of the IEEE conference on computer vision and pattern recognition*. 109–117.
- [31] Ashish Vaswani, Noam Shazeer, Niki Parmar, Jakob Uszkoreit, Llion Jones, Aidan N Gomez, Łukasz Kaiser, and Illia Polosukhin. 2017. Attention is all you need. *Advances in neural information processing systems* 30 (2017).
- [32] Orlin Wagner. 2022-06-15. Nearly 400 car crashes in 11 months involved automated tech, companies tell regulators. *National Public Radio* (2022-06-15). <https://www.npr.org/2022/06/15/1105252793/nearly-400-car-crashes-in-11-months-involved-automated-tech-companies-tell-regul>
- [33] Sanghyun Woo, Jongchan Park, Joon-Young Lee, and In So Kweon. 2018. Cbam: Convolutional block attention module. In *Proceedings of the European conference on computer vision (ECCV)*. 3–19.
- [34] Ye Xia, Jinkyu Kim, John Canny, Karl Zipser, Teresa Canas-Bajo, and David Whitney. 2020. Periphery-fovea multi-resolution driving model guided by human attention. In *Proceedings of the IEEE/CVF Winter Conference on Applications of Computer Vision*. 1767–1775.
- [35] Ye Xia, Danqing Zhang, Jinkyu Kim, Ken Nakayama, Karl Zipser, and David Whitney. 2018. Predicting driver attention in critical situations. In *Asian conference on computer vision*. Springer, 658–674.

- [36] Fisher Yu, Haofeng Chen, Xin Wang, Wenqi Xian, Yingying Chen, Fangchen Liu, Vashisht Madhavan, and Trevor Darrell. 2020. BDD100K: A Diverse Driving Dataset for Heterogeneous Multitask Learning. In *The IEEE Conference on Computer Vision and Pattern Recognition (CVPR)*.